

Elastic Anomaly of Helium Films at a Quantum Phase Transition

T. Makiuchi,¹ M. Tagai,¹ Y. Nago,¹ D. Takahashi,² and K. Shirahama¹

¹*Department of Physics, Keio University, Yokohama 223-8522, Japan*

²*Center for Liberal Arts and Sciences, Ashikaga University, Ashikaga 326-8558, Japan*

(Dated: November 7, 2018)

Helium films show various quantum phases that undergo quantum phase transitions by changing coverage n . We found anomalous elastic phenomena in bosonic ^4He and fermionic ^3He films adsorbed on a glass substrate. The films stiffen under AC strain at low temperature with an excess dissipation. The onset temperature of the stiffening decreases to 0 K as n approaches a critical coverage n_c . The elastic anomaly is explained by thermal activation of helium atoms from the localized to extended states with a distributed energy gap. We determine for the first time the energy band structure of helium films from elasticity. The ground states of ^4He and ^3He at $n < n_c$ are identically gapped and compressible, which are possibly a sort of Mott insulator or Mott glass.

PACS numbers: 05.30.Rt, 64.70.Tg, 67.25.bh, 67.25.dj, 67.30.ej, 68.60.Bs

I. INTRODUCTION

Quantum phase transition (QPT) has been actively studied in condensed matter physics, because it occurs between emergent quantum phases¹. In particular, superfluid– and superconductor–insulator transitions in superconducting films² and ultracold atoms in optical potentials^{3,4} are typical examples of QPTs. In superfluid–insulator QPTs, while superfluid phases are unique and well understood, there are various possibilities for insulating phases because they are determined by competition between quantum fluctuations, interparticle correlation, and external potential. In spatially periodic systems such as bosons in optical lattices, the insulating phase is Mott insulator. In disordered metals and atoms in disordered potentials, Anderson insulator and Bose glass are the candidates for insulating phases. In this paper, we propose that helium films offer a new example of QPT between a superfluid and a novel insulating phase, which has an energy gap and a finite compressibility.

Helium (bosonic ^4He and fermionic ^3He) films formed on solid substrates by adsorption undergo various QPTs between competing phases by changing coverage n (areal density) as an external parameter. On atomically flat surface of graphite, helium films form clear layer structures from one to several atomic layers⁵. Potential corrugation provided by graphite and correlation between helium atoms produce various ordered phases such as Mott insulator, heavy Fermi fluid, nuclear magnetic phases, and coexistence of superfluid and density wave order^{6–8}. On disordered substrates, such as glass and Mylar (plastic film), the situation is quite different. No clear layer structure is observed, and superfluidity emerges when n exceeds a critical value n_c , which is 6–27 $\mu\text{mol}/\text{m}^2$ (about 0.5–2 atomic layers) depending on substrates^{9,10}. The superfluid transition temperature T_c increases as n increases from n_c , while films at $n < n_c$ do not exhibit superfluidity. The superfluid films undergo a well-known Berezinskii–Kosterlitz–Thouless (BKT) transition on Mylar substrate¹¹, while films in porous media show

both two and three-dimensional characteristics due to the macroscopic connectivity of locally two-dimensional films^{12,13}.

The most important feature of ^4He films on disordered substrates is that there is only one “quantum critical coverage” n_c . Films at $n < n_c$ are considered to be in an insulating phase, meaning that a superfluid–insulator QPT occurs at n_c . We emphasize that ^4He on disordered substrates realizes an *ideal* superfluid–insulator QPT. On graphite, ^4He superfluidity and ^3He magnetism are strongly influenced by corrugation from substrate. It is rather surprising that superfluid transition of ^4He on Mylar shows a perfect agreement with the BKT theory¹¹, while ^4He on graphite does not¹⁴.

The existence of n_c was initially explained by the so-called inert layer model^{15,16}. In this model, an “inert” solid layer adjacent to substrate and a superfluid layer atop the inert layer form two independent subsystems. Although this model is consistent with the fact that n_c depends on helium–substrate potential depth, it does not explain the deviation of n – T_c relation from linearity, and the nonadditivity of heat capacity⁹. It is therefore desirable to study nature of the localized state and the QPT beyond the inert layer model.

Fisher *et al.* proposed that many-body effects of correlation and disorder make ^4He film at $n < n_c$ localized to be a Bose glass, which is characterized by no gap and finite compressibility¹⁷. But no evidence for the Bose glass of ^4He film was found experimentally¹⁰. We have found anomalous behavior in elasticity of helium films, an important property that is related to a compressibility of ground state. The ground state at $n < n_c$ is found to be a gapped many-body state such as Mott insulator or Mott glass¹⁸, which has intermediate properties between Mott insulator and Bose glass.

Contrary to ^4He , studies of ^3He films on disordered substrates were few. Since ^3He films show no superfluidity at currently available low temperatures and the heat capacity is dominated by a contribution from nuclear spins¹⁹, critical coverage n_c was not identified for ^3He . Also in ^3He films, we have observed the elastic anomaly

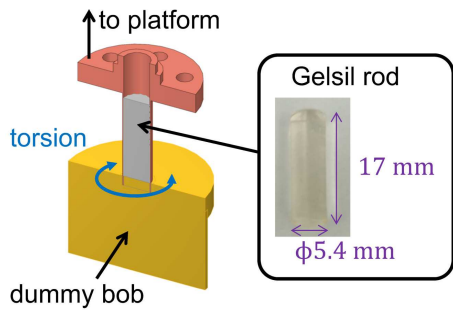


FIG. 1. A cross-sectional view of the torsional oscillator. The uppermost part has screw holes for mounting on a platform. The photograph shows the rod sample of porous Gelsil glass we have employed in this work.

identical to that of ^4He films. The critical coverage n_c is identified for the first time for ^3He .

II. EXPERIMENTAL METHOD

A. Torsional oscillator and porous glass

We have measured elasticity of helium films using a torsional oscillator (TO) shown in Fig. 1. Contrary to TO conventionally used in studies of superfluid helium, in which space for helium is located in the bob to measure mass decoupling, our present TO consists of a beryllium copper (BeCu) torsion rod containing a porous Gelsil glass sample and a brass dummy bob, which also acts as an electrode for torsional oscillation. Gelsil is a nanoporous silica glass manufactured by sol-gel method, and has nanopores that are randomly connected. Its structure is similar to that of porous Vycor glass, which was typically used in many superfluid helium studies. Adsorbed helium atoms form a film on the pore wall, and the atoms in fluid state can move along the wall. The Gelsil sample we used is cylindrical shape, 17 mm in length, and 5.4 mm in diameter. Before the construction of the TO, the Gelsil sample was baked at 150 °C in vacuum for 3 hours to eliminate adsorbed molecules, especially water. The sample mass after the baking was 0.371 g. Then we took a nitrogen adsorption–desorption isotherm at 77 K for surface characterization. A surface area analyzed with Brunauer–Emmett–Teller method²⁰ is 166 m² (447 m²/g). A pore diameter distribution, analyzed with Barrett–Joyner–Halenda²¹ method, has a peak at 3.9 nm. This peak pore size is larger than the nominal pore diameter 2.5 nm, which was determined by manufacturer. The Gelsil was again baked for 6 hours, and glued into the BeCu tube (6.0 and 5.5 mm in outer and inner diameter, respectively) with Stycast 1266 epoxy in a ^4He atmosphere. The TO was mounted on a torsional vibration isolator consisting of a massive copper platform with large rotational moment of inertia (70 mm ϕ , 30 mm thick) and a copper torsion rod (5 mm ϕ , 30 mm long).

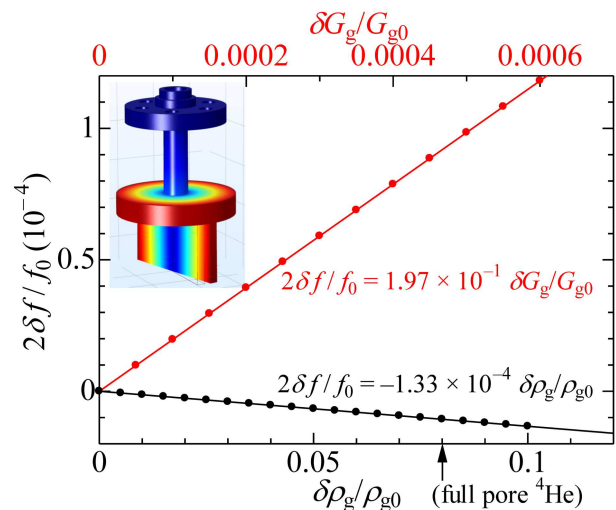


FIG. 2. Calculated frequency shift due to changes in the density ρ_g and in the shear modulus G_g of the Gelsil sample by FEM simulation. A possible maximal value of $\delta\rho_g/\rho_{g0}$ in the case of full-pore ^4He is indicated with an arrow. Inset is a false color picture indicating the movement of parts of our TO.

Two brass electrodes, which are for driving and detecting the torsional oscillation, are located on the platform so as to form two parallel plate capacitors with the flat faces of the dummy bob.

The whole TO setup was attached to a cold plate under a mixing chamber of a Joule–Thomson cooled dilution refrigerator (Cryoconcept Inc.). Sample temperature was measured using a RuO₂ thermometer (below 43 mK) and a calibrated germanium thermometer (43 mK–5 K) on the platform. The temperature was controlled with a Manganin twisted wire heater and the RuO₂ thermometer.

B. Finite element method

For the present TO, the resonant frequency of the torsion mode is simply given by $f = (1/2\pi)\sqrt{k/I}$, where k is a torsion constant (stiffness) of the rod and I is a moment of inertia of the dummy bob. As I is constant, an increase in f by changing the coverage indicates stiffening of adsorbed film. Rigorously, however, adsorption of helium on the porous Gelsil glass may slightly contribute to the moment of inertia of the bob, therefore the effects of both stiffening and mass loading should be investigated.

We performed simulations with finite element method (FEM) to compute how much the resonant frequency of the current TO changes by effective stiffening and mass loading of the Gelsil sample after helium adsorption. We treat the Gelsil rod as a continuous material with a Young’s modulus $E = 17.1$ GPa and a Poisson’s ratio $\nu = 0.155$, measured by an ultrasound measurement²². The calculated resonant frequency by FEM was $f_0 = 962$

Hz for the present TO, which is about 10 percent larger than the measured value $f_0 = 860$ Hz at low temperatures. The origin of this difference in f_0 is not known. One possible reason is that the inhomogeneity of silica structure in the porous glass sample, which is not taken into account in the FEM but might affect the resonant frequency in reality. The reduced resonant frequency shift $2\delta f/f_0$, however, is a good quantity to compare the measured value to the FEM result.

If the adsorbed helium film stiffens, the apparent shear modulus of Gelsil substrate G_g will increase, i.e. $G_g \rightarrow G_{g0} + \delta G_g$. Helium adsorption also increases the apparent density of Gelsil, i.e. $\rho_g \rightarrow \rho_{g0} + \delta\rho_g$. The frequency changes for small $\delta G_g/G_{g0} = \delta E/E$ and $\delta\rho_g/\rho_{g0}$ are well fitted by linear functions as shown in Fig. 2. The results are

$$\frac{2\delta f}{f_0} = 1.97 \times 10^{-1} \frac{\delta G_g}{G_{g0}}, \quad (1)$$

and

$$\frac{2\delta f}{f_0} = -1.33 \times 10^{-4} \frac{\delta\rho_g}{\rho_{g0}}. \quad (2)$$

The effect of elasticity is larger than that of mass loading by a factor of 10^3 in the present TO.

The effective density change in the Gelsil due to helium adsorption is

$$\frac{\delta\rho_g}{\rho_{g0}} = \frac{mnN_A S}{m_{g0}} \leq \frac{p\rho_{\text{liq}}}{\rho_{g0}}, \quad (3)$$

where m is mass of a helium atom, n the coverage, N_A Avogadro's constant, and ρ_{liq} the density of bulk liquid helium. $S = 166$ m², $m_{g0} = 0.371$ g, $p = 0.54$, and $\rho_{g0} = 0.954$ g/cm³ are the surface area, the mass, the porosity, and the density of the Gelsil sample, respectively. For example, $n = 23$ $\mu\text{mol}/\text{m}^2$ of ⁴He film gives $\delta\rho_g/\rho_{g0} = 0.041$ and $2\delta f/f_0 = -5.5 \times 10^{-6}$. Even if the pores are filled with liquid ⁴He, it gives $\delta\rho_g/\rho_{g0} = p\rho_{\text{liq}}/\rho_{g0} = 0.08$, hence $2\delta f/f_0 = -1 \times 10^{-5}$. Therefore, if we measure a frequency increment greater than $2\delta f/f_0 \sim 1 \times 10^{-5}$ ($\delta f \sim 4$ mHz) for any coverage of ⁴He or ³He, it is explained by changes in elasticity. Mass decoupling by the superfluid and ‘‘supersolid’’ transitions and by slippage phenomenon²³ is excluded from the origin.

C. Experimental procedure

We first performed the measurement for ⁴He films. Then the TO was warmed up to room temperature to get rid of ⁴He, and the measurement for ³He was made. For each run, the resonant frequency and energy dissipation of the TO without helium film were measured at first.

The TO was forced to oscillate electrostatically at the resonant frequency f using a loop circuit. The driving was made by applying a pulsed voltage of 1.5 V and

a width of 50 μs , with dc bias voltage 200 V_{dc}, which was applied to the dummy bob electrode. In this condition, the strain applied to Gelsil rod is estimated to be 1.6×10^{-7} , and the maximal velocity at the Gelsil rim near the dummy bob is 15 $\mu\text{m}/\text{s}$. We confirmed that the oscillation amplitude is linear to the drive voltage around this condition. The resonant frequency f was measured by a frequency counter stabilized by a rubidium frequency standard.

The dissipation Q^{-1} was taken from the current R due to capacitive change measured by a lock-in amplifier. After the drive voltage is stopped, R decreases exponentially with time; $R(t) = R_0 e^{-t/t_0}$, where t_0 is a relaxation time. The inverse of the dissipation gives Q factor of oscillation, which is $Q = \pi f t_0$. The Q factor is proportional to the current at a drive, $Q = cR$, and the constant c was measured before the warming and after the cooling at the lowest temperature for each coverage. We confirmed that c does not change during a run. For the ⁴He run, $c = 2.48 \times 10^{13}$ A⁻¹, and for the ³He run, $c = 2.06 \times 10^{13}$ A⁻¹. The dissipation Q^{-1} at each temperature is obtained from the corresponding current R .

We refer to the temperature dependencies of f and Q^{-1} without helium ($n = 0$, empty cell) as the background. The resonant frequencies of the TO at $n = 0$ and at 1.0 K were $f_0 = 860.822$ Hz for ⁴He and $f_0 = 860.145$ Hz for ³He run. The slight difference between two runs was by a thermal cycle. Fig. 3 shows the resonant frequency f from which a constant f_0 is subtracted and the energy dissipation Q^{-1} of $n = 0$ for the ⁴He and ³He runs as a function of temperature. The frequency was found to be linear in $\log(T/\text{K})$ at $T > 20$ mK. We fit f by

$$f(T, n = 0) = \sum_{i=0}^1 A_i [\log(T/\text{K})]^i. \quad (4)$$

The fitting results are shown in Fig. 3. For the ³He run, f takes a maximum at about 30 mK and decrease with further lowering T , probably by the effect of tunneling two-level systems (TLS) in the glass sample²⁴. We assume that f is constant below 30 mK because the number of data are not sufficient to fit the T dependence.

The dissipation Q^{-1} slightly increases as T decreases from 1 K to 80 mK, followed by a sudden drop below 50 mK. We fit Q^{-1} by polynomial

$$\log[Q(T, n = 0)] = \sum_{i=0}^9 B_i [\log(T/\text{K})]^i. \quad (5)$$

For preparing an adsorbed helium film, a known amount of helium gas was admitted from a room temperature gas-handling system with 1 L standard volume to the TO at $T < 150$ mK. We have used commercial G1 grade ⁴He gas with impurity concentration less than 5×10^{-7} , and ³He gas with nominal purity 99.95 %. After adsorbing helium gas at low temperature, the TO was warmed up at sufficiently high temperature, typically 1–5 K, for several hours to uniformly spread out in the Gelsil.

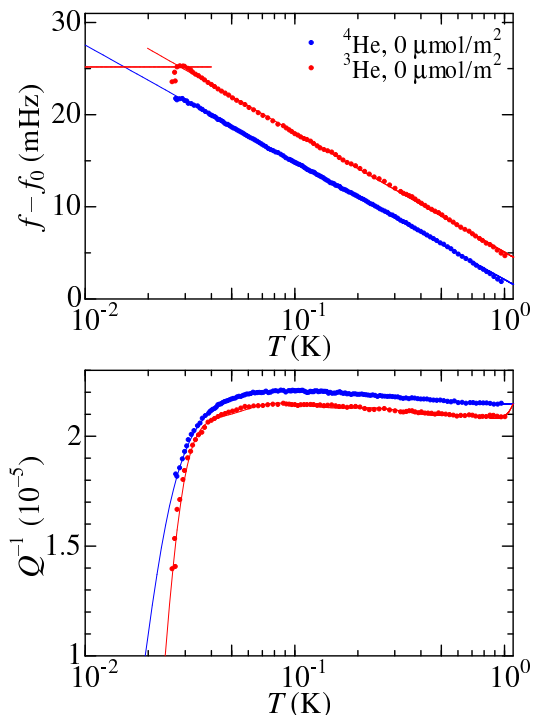


FIG. 3. The background data of the empty cell. The upper panel is the resonant frequency f from which a constant f_0 is subtracted. Here $f_0 = 860.82$ Hz for the ^4He run, and $f_0 = 860.14$ Hz for the ^3He run. The lower panel is the dissipation Q^{-1} for the ^4He and ^3He runs. Lines are results of the fitting (see text).

The TO was again cooled to 10–30 mK and then warmed up to 1.1 K to measure the temperature dependence of the resonant frequency f and the dissipation Q^{-1} . Data shown in this paper were taken during the warming. The warming was done with PID control of the heater power while the dilution refrigerator was properly operated. After the warming, the heater was turned off and the TO was cooled, and adsorption for the next coverage was started. No hysteresis was observed in the data between the warming and cooling.

The annealing temperature and duration were selected so that the frequency and the amplitude become stable. For ^4He films of coverage $n < 15 \mu\text{mol}/\text{m}^2$, the annealing was done at 5 K for 5 hours. At $16 \leq n \leq 26 \mu\text{mol}/\text{m}^2$, it was done at 1.1 K for more than 14 hours. For ^3He films, we annealed at 5 K for 5 hours for all coverages. For $16 \mu\text{mol}/\text{m}^2$ of ^3He , we first annealed at 1.1 K for 12 hours as in the case of ^4He film. However, this condition was not sufficient because the frequency and dissipation were almost the same as those of previous $n = 15 \mu\text{mol}/\text{m}^2$ data. This indicates that ^3He atoms in the extended state (see later section) are less mobile than ^4He atoms. We finally found that the annealing at 5 K for 5 hours was sufficient for ^3He .

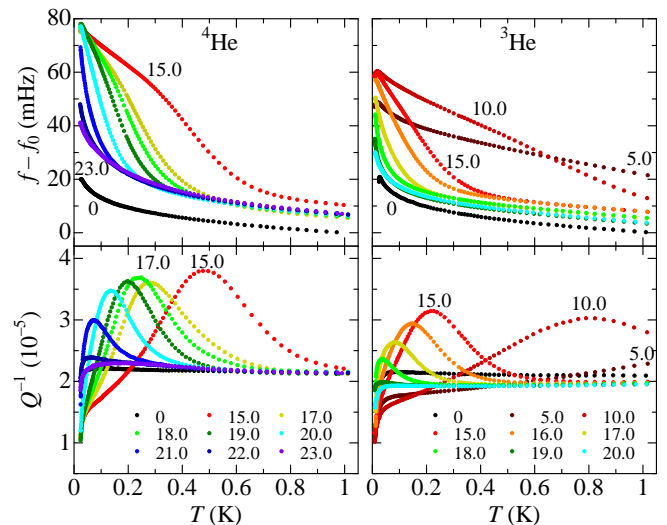


FIG. 4. The resonant frequency f and dissipation Q^{-1} of the TO for ^4He (left) and ^3He films (right). Numbers give the coverage n in unit of $\mu\text{mol}/\text{m}^2$. Correspondence between f and Q^{-1} is shown by colors of data. All the f data are shown after subtracting a constant frequency f_0 , which is 860.822 Hz for ^4He and 860.145 Hz for ^3He , respectively.

III. RESULTS AND DISCUSSION

A. Raw data

In Fig. 4, we show raw data for the coverage n from 0 to $23 \mu\text{mol}/\text{m}^2$ for ^4He , and to $20 \mu\text{mol}/\text{m}^2$ for ^3He , respectively. The dots in black are the background ($n = 0$). Helium adsorption ($n > 0$) increases f in the entire temperature range from the background.

At each coverage, f increases as T decreases more rapidly than the background does. By comparing the data with FEM simulations, we find that the observed increase in f is originated from change in elasticity of helium adatoms. The FEM simulation shows that if $15 \mu\text{mol}/\text{m}^2$ of ^4He were decoupled from the oscillation, f would increase by 1.5 mHz, which is nearly two orders of magnitude smaller than the observed increment at lowest T , $\delta f \sim 50$ mHz. Therefore, the increase in TO frequency is not due to the change in mass loading, i.e. superfluidity, supersolidity and slippage of helium films, but is originated from stiffening of helium films.

The dissipation Q^{-1} has a peak at a temperature where the slope of f is the largest, and its position decreases with increasing n . As T decreases further, f tends to saturate and Q^{-1} decreases. These behaviors of $f(T)$ and $Q^{-1}(T)$ are qualitatively the same for ^4He and ^3He films. We call these phenomena *elastic anomaly*. The elastic anomaly vanishes at $n \simeq 23$ and $20 \mu\text{mol}/\text{m}^2$ for ^4He and ^3He , respectively. We can regard these coverages as the critical coverage n_c . We will discuss later that n_c determined from the elastic anomaly in ^4He is identical to

n_c for the onset of superfluidity within the experimental accuracy. At coverages $n > n_c$, both $f(T)$ and $Q^{-1}(T)$ are almost identical to those of the $n = 0$ background, except for small upward shift in f at all temperatures (+6 and +3 mHz for ^4He and ^3He , respectively). Therefore, in the superfluid phase of ^4He and liquid phase of ^3He , no prominent elastic anomaly is observed. It is remarkable that at $n > n_c$ the TO behaves as if there were no adsorbed helium except the temperature-independent shift.

The gradual increase in f suggests a crossover of helium film from a soft to a stiff state, not a first order phase transition such as solidification.

Comparing the resonant frequencies at $n = 15$ and $23 \mu\text{mol}/\text{m}^2$ of ^4He , for instance, we see that $f(15 \mu\text{mol}/\text{m}^2)$ is larger than $f(23 \mu\text{mol}/\text{m}^2)$ in the entire temperature range. This means that the thinner film has a *larger* elastic constant than the thicker film does. Such a coverage dependence of elastic anomaly can never be explained by the inert layer model. We show below that a two-band model considering gapped excitation in the localized state explains qualitatively the observed elastic anomaly.

B. Anelastic model and energy gap

The temperature dependencies of f and Q^{-1} are typical of a relaxational crossover between a soft state at high T and a stiff state at low T under AC stress applied to a substrate-He system. Assuming that the relaxation is caused essentially by adsorbed helium, the relaxational contribution to f and Q^{-1} is obtained by subtraction of the background from the raw data. We define the frequency shift by

$$\delta f \equiv f(T, n) - f(T, 0) - [f(1 \text{ K}, n) - f(1 \text{ K}, 0)]. \quad (6)$$

By this definition, we have omitted the background and the small constant frequency increments which were seen for all coverages (see f at high temperatures), so as to set $\delta f = 0$ at 1.0 K. The temperature-independent extra background is attributed to adsorption of atoms in particularly deep potential sites on the disordered substrate, and this omission was necessary for the fitting of data to the response function given later. We also define the excess energy dissipation by

$$\delta Q^{-1} \equiv Q^{-1}(T, n) - Q^{-1}(T, 0). \quad (7)$$

This definition was sufficient for the data of ^4He , but we have added a small constant to set $\delta Q^{-1}(1 \text{ K}) = 0$ for the data of ^3He .

Figure 5 shows a normalized frequency shift $2\delta f/f_0$ and an excess dissipation δQ^{-1} for ^4He at $n = 18 \mu\text{mol}/\text{m}^2$. Other data, including ^3He data, are presented in Figs. 9 and 10 in Appendix. The dissipation δQ^{-1} becomes negative below 0.1 K, meaning that helium adsorption decreases the internal loss of the glass.

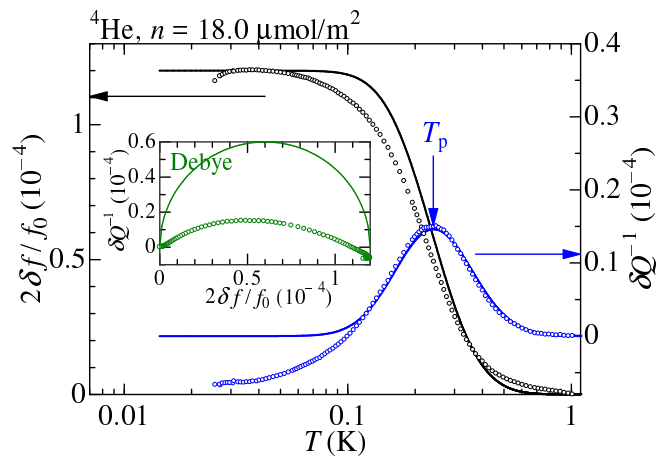


FIG. 5. The normalized resonant frequency $2\delta f/f_0$ and excess dissipation δQ^{-1} for a ^4He film at $n = 18 \mu\text{mol}/\text{m}^2$. Solid curves are the results of fitting to the response function, Eq. (11). Fitting parameters are as follows: $\delta G/G_0 = 1.20 \times 10^{-4}$, $\tau_0 = 0.4 \text{ ns}$, $\Delta/k_B = 3.1 \text{ K}$, and $\sigma = 0.38$. A vertical arrow shows T_p . Inset is Cole-Cole plot of the data. Semicircle shows the Debye relaxation with a single τ .

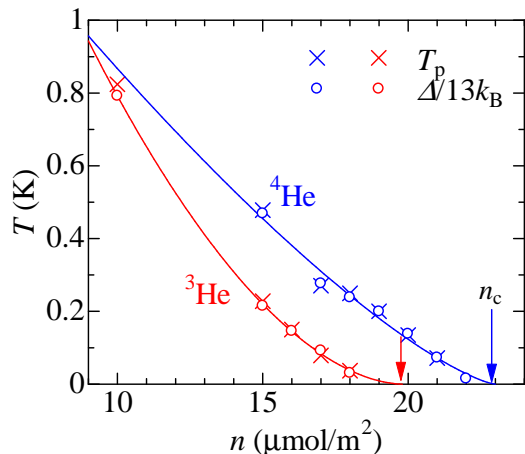


FIG. 6. The dissipation-peak temperature T_p , and the energy gap Δ obtained from the fittings as a function of the coverage. Solid curves are power law fits for Δ (see text). Arrows indicate critical coverage n_c .

The physical origin of this apparently negative dissipation has not been elucidated.

The dissipation-peak temperature T_p is indicated by an arrow in Fig. 5. It can be recognized as a crossover temperature between the stiff and the soft state. The coverage dependence of T_p is shown in Fig. 6. T_p approaches 0 K at $n = n_c$ with a concave curvature.

The relaxational crossover is explained by a thermal activation process of helium adatoms between two discrete energy bands^{10,25}. At $T = 0$, helium atoms are localized and forms an energy band. At finite temper-

atures, the localized atoms are thermally excited to another band of extended states separated by an energy gap. The excited atoms move freely along the substrate and act as a normal fluid. We analyze $2\delta f/f_0$ and δQ^{-1} by dynamic response functions for anelastic relaxation, according to similar anelasticity analysis for bulk solids²⁶

$$\frac{2\delta f(T)}{f_0} = \frac{\delta G}{G_0} \left[1 - \frac{1}{1 + [\omega\tau(T)]^2} \right], \quad (8)$$

$$\delta Q^{-1}(T) = \frac{\delta G}{G_0} \frac{\omega\tau(T)}{1 + [\omega\tau(T)]^2}, \quad (9)$$

where δG and G_0 are a relaxed shear modulus and a shear modulus of TO rod respectively, and $\omega = 2\pi f \simeq 2\pi f_0$. The dissipation δQ^{-1} has a peak at $\omega\tau = 1$. The thermal relaxation time is given by $\tau(T) = \tau_0 e^{E/k_B T}$, where E is an energy gap (an activation energy) and τ_0^{-1} is an attempt frequency. Now it becomes clear that the dissipation-peak temperature T_p is the temperature which holds $1 = \omega\tau_0 e^{E/k_B T_p}$.

If $\tau(T)$ were single valued, the relaxation would be a Debye type and the plot of $2\delta f/f_0$ versus δQ^{-1} would be a semicircle shown in the inset of Fig. 5. The plot is, however, a deformed semicircle, meaning that E has a distribution.

We assume a log-normal distribution for E

$$F(E) = \frac{1}{\sqrt{2\pi}\sigma E} \exp\left(-\frac{[\ln(E/\Delta)]^2}{2\sigma^2}\right), \quad (10)$$

where Δ is the median (a value separating the higher half of the population from the lower half). We hereafter regard Δ as the energy gap. The selection of a log-normal distribution is reasonable because $\delta Q^{-1}(T)$ is almost symmetric for $\log(T)$ scale as shown in Fig. 5. We obtain a complex form of the dynamic response function as

$$\frac{2\delta f}{f_0} + i\delta Q^{-1} = \frac{\delta G}{G_0} \left[1 - \int_0^\infty \frac{F(E)}{1 + i\omega\tau(E, T)} dE \right]. \quad (11)$$

We perform fittings of Eq. (11) to the data. The results are shown with solid curves in Fig. 5, and Figs. 9 and 10 in Appendix. Equation (11) fits well to the data, and the negative δQ^{-1} below 0.1 K does not give much influence to the quality of the fittings.

We find a remarkable relation between Δ and T_p , $\Delta \simeq 13k_B T_p$, for both ^4He and ^3He , as clearly shown in Fig. 6. This relation between Δ and T_p reinforces the validity of the fittings. Other fitting parameters, $\delta G/G_0$, τ_0 and σ , have no systematic dependencies on n . The inverse attempt frequency τ_0 is ranged from 0.4 to 0.6 ns, which holds the aforementioned relation $1 = \omega\tau \simeq \omega\tau_0 e^{13}$.

Figure 6 shows that Δ and T_p monotonically decrease with some scatters. The gap is fitted by a power law

$$\Delta = \Delta_0 |1 - n/n_c|^a. \quad (12)$$

Nonlinear fittings give $\Delta_0/k_B = 23.9$ K, $n_c = 23.0$ $\mu\text{mol}/\text{m}^2$ and $a = 1.32$ for ^4He , and 36.5 K, 19.8 $\mu\text{mol}/\text{m}^2$ and 1.80 for ^3He , respectively.

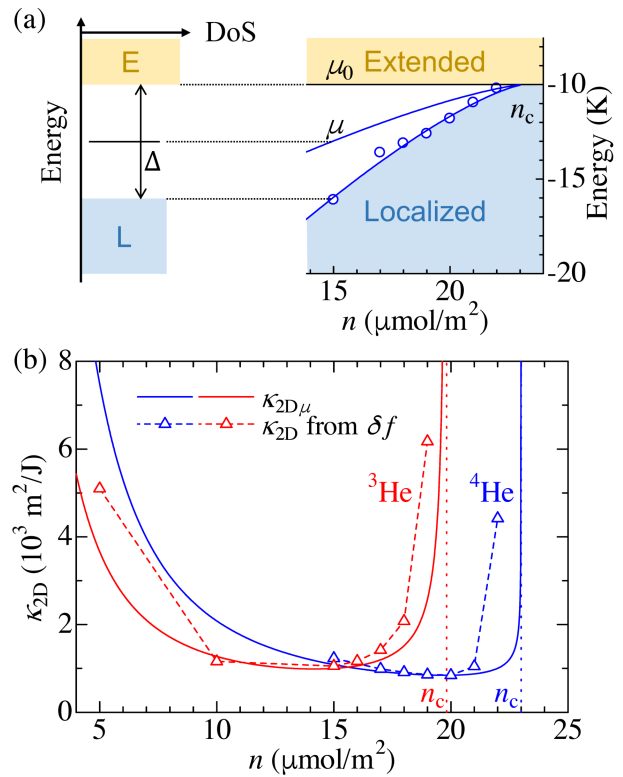


FIG. 7. (a) Proposed energy band for helium films. The left side shows density of states (DoS) of the localized and extended states separated by a gap Δ . The chemical potential μ is located at the middle of the gap. The right side shows its n dependence. The uppermost energy of the localized states increases with n , while the lowermost energy of the extended states stays at -10 K, which was obtained as the chemical potential of ^4He film on glass from a numerical study²⁷. (b) 2D compressibility of ^4He and ^3He films. Solid curves show $\kappa_{2D\mu}$ from Eq. (15) and triangles show κ_{2D} directly obtained from δf using Eq. (16).

C. Energy band and compressibility

The fact that Δ smoothly decreases to zero as $n \rightarrow n_c$ indicates that the energy band also smoothly changes with n . We propose an energy band in Fig. 7(a). The localized states are completely filled at $T = 0$, and its uppermost edge is determined by n . Atoms in the localized states contribute to the elasticity. On the other hand, the extended states are empty at $T = 0$, and their lowermost edge, μ_0 , has no or negligible dependence on n . At high T , helium atoms are thermally excited from the localized to the extended states, resulting a softening. At $n \geq n_c$, the gap is closed, and helium atoms can enter the extended states even at $T = 0$. ^4He atoms condensed in the extended states show superfluidity. This scenario was first discussed by Crowell *et al.* in a heat capacity study of ^4He films¹⁰.

The band for each n is analogous to that of intrinsic semiconductor. The chemical potential μ at $T = 0$ is a

function of n and is located at the middle of the gap, so that

$$\mu(n) = \mu_0 - \Delta(n)/2. \quad (13)$$

The 2D compressibility is, by definition,

$$\kappa_{2D\mu} = \left(N_A n^2 \frac{\partial \mu}{\partial n} \right)^{-1}, \quad (14)$$

where N_A is the Avogadro constant ($N_A n$ is a 2D number density of atoms). We refer to the 2D compressibility obtained from $\mu(n)$ as $\kappa_{2D\mu}$. From Eqs. (12), (13) and (14), we get

$$\kappa_{2D\mu} = \frac{2n_c}{aN_A n^2 \Delta_0} |1 - n/n_c|^{1-a}. \quad (15)$$

The results are drawn in Fig. 7(b) with solid curves.

The 2D compressibility is also obtained by directly comparing the observed frequency increment $\delta f(n)$ with Eq. (1), the FEM result. Here $\delta f(n)$ is frequency increment from $f(n_c)$ at the lowest temperature. We use $f(n_c)$, not $f(n=0)$, as the reference value because $f(n_c)$ contains the elastic contribution from atoms in deep potential sites which we want to exclude from the calculation. The shear modulus of Gelsil is $G_{g0} = 7.38$ GPa from an ultrasound study²². With a general relation $K = \lambda + (2/3)G$, where K is a bulk modulus and λ is a Lámé constant, an effective 3D compressibility of helium film κ is $\kappa^{-1} = \delta K \simeq (2/3)\delta G$. It is converted to the 2D compressibility by $\kappa_{2D} = \kappa/d$, where $d = v_{\text{film}}n$ is mean film thickness and v_{film} is molar volume of helium film. Since v_{film} is unknown, we employ v of liquid helium at 0 bar, which might be larger than v_{film} . Combining these equations, we have

$$\kappa_{2D} = \frac{0.148f_0}{\delta f(n)G_{g0}vn}. \quad (16)$$

In Fig. 7(b), we plot κ_{2D} obtained from Eq. (16). The overall agreement between $\kappa_{2D\mu}$ and κ_{2D} from δf definitely assures the proposed band. In both ^4He and ^3He , κ_{2D} first decreases, then makes a plateau, and finally shows divergent behavior as n approaches n_c .

D. Phase diagram

The universality in ^4He and ^3He films is revealed by constructing a “unified” phase diagram shown in Fig. 8. The peak temperatures T_p 's of ^4He and ^3He as a function of n/n_c nearly collapse onto each other, except that the curvatures differ. The difference of the zero-point energy, hence the binding energy from the substrate, between ^4He and ^3He does not affect the magnitude of the characteristic temperatures of the elastic anomaly.

Superfluid transition temperatures T_c 's of ^4He on Gelsil in a previous TO study²⁸ are also plotted in Fig.

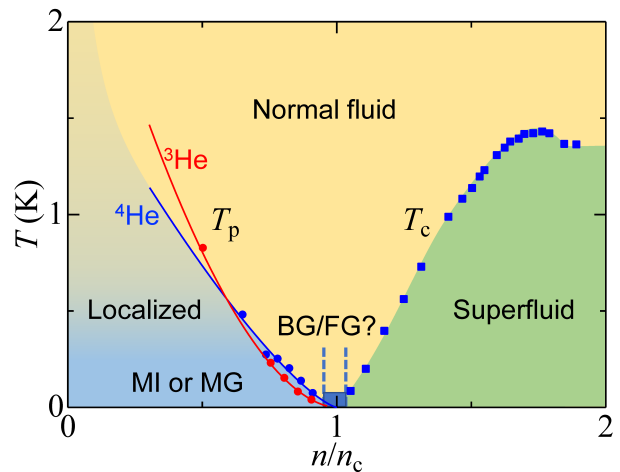


FIG. 8. A unified phase diagram constructed by crossover temperature T_p and superfluid transition temperature T_c (only for ^4He) as a function of n/n_c . The superfluid transition temperature is from previous TO study²⁸ (^4He on Gelsil, $n_c = 20 \mu\text{mol}/\text{m}^2$). The peak temperature divides the localized phase from normal fluid phase. The localized phase near $T = 0$ is a sort of Mott insulator (MI) or Mott glass (MG). Possible region for Bose glass (BG) or Fermi glass (FG) is shown.

8. The critical coverage for it was inferred to be $n_c = 20 \mu\text{mol}/\text{m}^2$, which is slightly smaller than $23 \mu\text{mol}/\text{m}^2$ for the elastic anomaly. The nominal pore diameters were 2.5 nm for both porous Gelsil samples, but they were provided by different manufacturers. The discrepancy in n_c might be originated from differences in some characteristics such as residual impurities, pore size and its distribution between two samples.

In a previous TO study, a TO with a Gelsil in the bob (named TO1, see Appendix B) has detected both the superfluid transition and the elastic anomaly, the latter is confirmed by the present study. The two characteristic temperatures, T_p and T_c , meet at the same critical coverage $n_c = 22 \mu\text{mol}/\text{m}^2$ in the experimental resolution (see Fig. 13 in Appendix B). A heat capacity study by Crowell *et al.*¹⁰ may also suggests the common critical coverage for “ T_B ” and T_c , though the physical meaning of T_B , a crossover temperature of the heat capacity at $n < n_c$, is not clear. Further experimental studies in the vicinity of n_c is necessary to conclude that the n_c 's of the superfluidity and the elastic anomaly are exactly identical or slightly different.

Figures 6 and 8 show that $\Delta(n)$ and T_p obey a power law $\Delta \propto T_p \propto |n - n_c|^a$ with $a > 1$. A symmetry may exist between the critical exponent of Δ and that of superfluid T_c of ^4He films, in which $T_c \propto (n - n_c)^w$ with $w > 1$ in all previous results^{9,10}.

Our finding is that ^4He and ^3He films at $n < n_c$ are identically *gapped* and *compressible* irrespectively of quantum statistics. These features do not strictly agree with the properties of Bose glass (gapped, compressible,

for ^4He ¹⁷, Mott insulator (gapped, incompressible) or Mott glass (single-particle gap, incompressible)¹⁸.

We propose, however, that the localized helium film is a sort of Mott insulator or Mott glass in a realistic situation. One may consider the following model: Helium atoms are first adsorbed on some particularly deep adsorption sites, so as to weaken randomness. Additional helium atoms are adsorbed on the weakened potential surface, and self-organize a nearly spatially periodic 2D Mott insulator or Mott glass with an n -dependent lattice spacing. The self-organization of sites allows a finite compressibility. The gap is finite because “sites are fully occupied” and an atom needs a finite energy to move.

Tackling this problem is important because it is related the nature of the onset of superfluidity, the quantum critical phenomena and the boson and fermion localization. Theoretical, numerical, and more experimental works are desired.

The gapped localized state which terminates at a certain coverage (n_c) has been observed in helium films on various substrates, such as Vycor^{10,25}, Hectorite (2D flat substrate), FSM (1D pores), and zeolites²⁹. This suggests that the gapped localized Mott insulator or Mott glass ubiquitously exists, irrespectively of substrate randomness and dimensionality.

As to the ^4He films, our result does not reject possibility of Bose glass in the vicinity of $n = n_c$, where the gap is almost closed and the compressibility significantly increases. Theories predict Bose glass emerging between Mott insulator and superfluid in the presence of moderate disorder¹⁷. The previous experiment discussed a quantum critical behavior of possible Bose glass near n_c ¹⁰. In our system, Bose glass can exist at about $22 < n < 23 \mu\text{mol}/\text{m}^2$, and a corresponding Fermi glass can occur in ^3He at $19 < n < 20 \mu\text{mol}/\text{m}^2$. Recently, QPTs among Mott insulator, Mott glass, Bose glass and Bose-Einstein condensate are realized in a quantum magnet³⁰. Helium films in disordered substrates can open a new perspective of QPTs for advantage of variable correlation and quantum statistics.

IV. CONCLUSIONS

We have discovered that the localized ^4He and ^3He films on a porous glass show an identical elastic anomaly. The elastic anomaly is explained by thermal activation of helium atoms from the localized to extended states with a distributed energy gap, which decreases as the film approaches the critical coverage n_c . The two-dimensional compressibility showed divergent behavior near n_c , which was deduced from the power law behavior of the gap and the energy band. The divergent behavior of the compressibility was confirmed from the direct calculation of the observed frequencies. Both the localized ^4He and ^3He are gapped and compressible, suggesting that the ground state is a sort of Mott insulator or Mott glass. Future studies in the vicinity of n_c at lower temperatures will

unveil the nature of the QPT.

ACKNOWLEDGMENTS

We thank M. Kobayashi, T. Ohtsuki and A. J. Beekman for useful discussions, and T. Kogure, H. Yoshimura, R. Higashino and Y. Shibayama for the previous torsional oscillator study using TO1 in Appendix. This work was supported by JSPS KAKENHI Grant Number JP17H02925. TM was supported by Grant-in-Aid for JSPS Research Fellow 18J13209, Research Grant of Keio Leading-edge Laboratory of Science and Technology, and Keio University Doctorate Student Grant-in-Aid Program.

Appendix A: Additional data for the fittings

We show in Figs. 9 and 10 additional data from which the background is subtracted. The results of fittings to Eq. (11) are also shown.

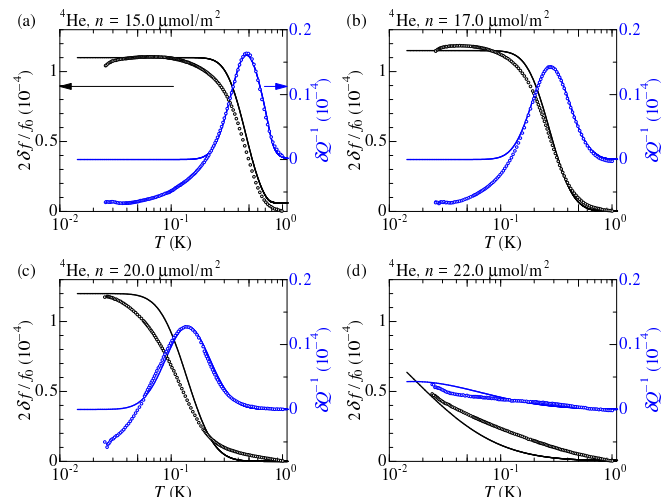


FIG. 9. The normalized resonant frequency $2\delta f/f_0$ and excess dissipation δQ^{-1} for ^4He films at several coverages. Solid lines are the results of fitting to the complex response functions with a log-normal distributed energy gap (see text).

Appendix B: Interpretation of standard torsional oscillator experiments

Our direct elasticity measurement was motivated by the observation of frequency shift and excess dissipation in a torsional oscillator for the study of superfluid properties of ^4He films in porous Gelsil glass. Here we briefly discuss the results and interpretation in the previous TO studies.

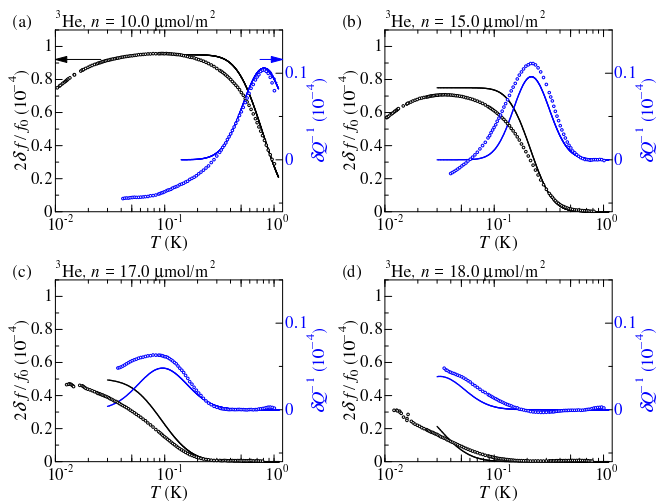


FIG. 10. The normalized resonant frequency $2\delta f/f_0$ and excess dissipation δQ^{-1} for ^3He films at several coverages. Solid lines are the results of fitting to the complex response functions with a log-normal distributed energy gap (see text).

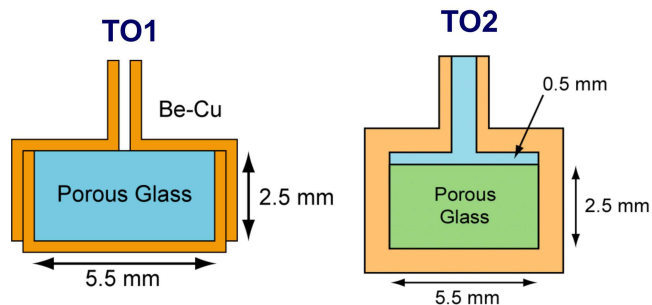


FIG. 11. Schematic cross sectional views of TO1 and TO2. The porous glass sample is glued to the BeCu enclosure with epoxy.

Two TOs, which we refer to as TO1 and TO2, were employed as shown in Fig. 11. Each TO contained a disk sample of porous Gelsil glass inside the torsion bob. In TO1, we glued all the faces of the glass sample to the wall by Stycast 1266 epoxy. The epoxy penetrated to the hole of the torsion rod was carefully removed by inserting a drill bit. On the other hand, in TO2, there was an open space between the porous glass and one side of the wall of the bob, at which the torsion rod is attached.

We performed measurements of f and Q^{-1} of TO1 and TO2 with adsorbed ^4He at $6 < n < 35 \mu\text{mol}/\text{m}^2$. In TO1, we observed an increase in f accompanied by a dissipation peak at $n < 22 \mu\text{mol}/\text{m}^2$, as in the case of the present work. Figure 12 shows a result of fitting to the observation, which are converted to the normalized frequency shift $2\delta f/f_0$ and excess dissipation δQ^{-1} . We see that the overall T dependencies of TO1 are identical to the results of the present TO, in which the Gelsil sample is located in torsion rod. The fitting of the data to the

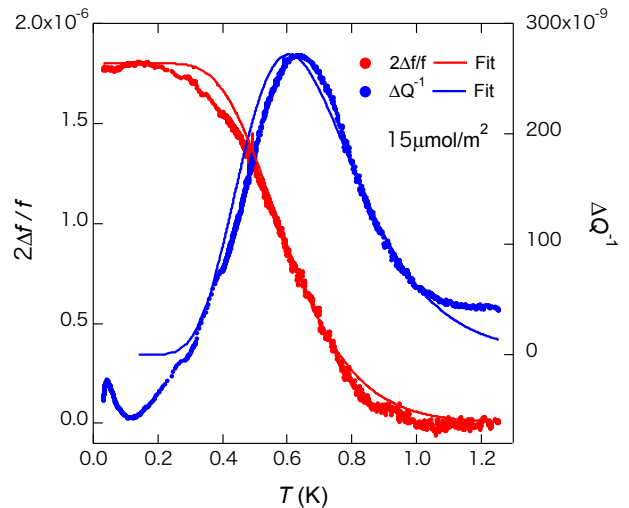


FIG. 12. Anomalous response observed in TO1 for ^4He coverage $n = 15.0 \mu\text{mol}/\text{m}^2$. The data shown are after subtracting the background from the raw data and normalized to $2\delta f/f_0$ and δQ^{-1} as in the main text. Note that the magnitude of effects is small by a factor of 10^{-2} compared with the present TO. Solid lines are the results of fitting similar to that described in the main text.

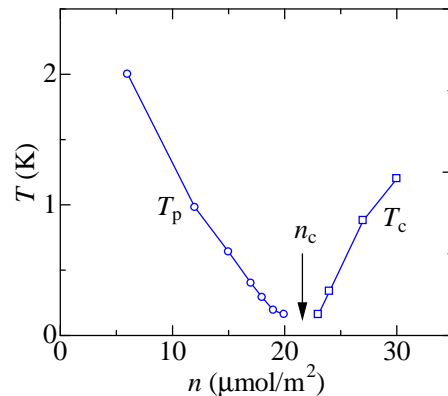


FIG. 13. The dissipation-peak temperature T_p and the superfluid transition temperature T_c of ^4He film detected with TO1. The arrow is at $n = 21.6 \mu\text{mol}/\text{m}^2$.

complex response functions described in the main text works well. We confirmed that in TO1 the dependence of the behaviors on n and the obtained fitting parameters such as energy gap Δ are also identical to the present TO. At $n > n_c$, ordinary superfluid transitions were observed as an increase in f below T_c . The dissipation-peak temperature T_p and the superfluid transition temperature T_c are plotted in Fig. 13. The critical coverages n_c determined from the n dependencies of T_p and T_c are identical within the accuracy of the data.

In TO2, however, such an elastic anomaly below n_c was not observed, while the superfluid transition was seen at $n > n_c$ as in TO1. The superfluid transition temperature T_c in Fig. 8 is from TO2²⁸. We have found that the absence of the elastic anomaly in TO2 is originated from

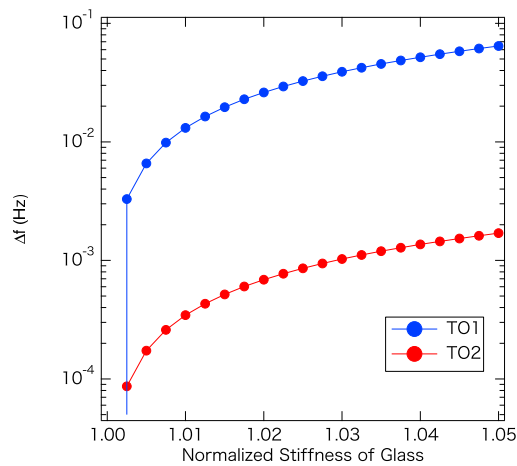


FIG. 14. Calculated change in resonant frequency, δf , as a function of normalized stiffness of porous glass sample in TO1 and TO2: e.g. the value 1.01 corresponds to the one percent increase in shear modulus of glass by adsorbed helium. Difference of about 40 times between the cases of TO1 and TO2 is seen.

the existence of open space between a face of porous glass disk and the wall of the TO cell near the torsion rod. We calculated the change in resonant frequency when the shear modulus of glass inside the TO bob increases,

assuming the structures of TO1 and TO2 in FEM simulations. The results are shown in Fig. 14. When the shear modulus of glass inside TO1 increases 5 percent, f increases about 60 mHz, while it increases only 2 mHz in TO2.

We interpret these results as follows: In a realistic TO made of metal for superfluid studies, the torsion bob is not rigid, and the resonant frequency of the fundamental torsion mode is determined not only by the shear modulus of the torsion rod but also by the shear modulus of the torsion bob, which consists of porous glass, BeCu enclosure and adsorbed helium in our experiments. This non-ideal nature of TO has been established by studies of apparent supersolidity of bulk solid ^4He using TOs with many different designs^{31–33}. In particular, it has been realized as the Maris effect that the stiffness of the part of TO near the torsion rod has a large contribution to resonant frequency³⁴. The presence of the elastic anomaly in TO1 and its absence in TO2 may be a manifestation of the Maris effect. In TO2, the stiffening of porous glass sample by helium adsorption will hardly contribute to the total torsion constant by the existence of open space inside the bob. We emphasize that this effect would be revealed only by FEM simulations, because it is difficult to calculate analytically the resonant frequency of a realistic TO with complicated structure and composites of different materials.

- ¹ S. Sachdev, *Quantum Phase Transitions*, 2nd ed. (Cambridge University Press, 2011).
- ² V. Dobrosavljevic, N. Trivedi, and J. V. James M., eds., “Conductor-insulator quantum phase transitions,” (Oxford University Press, 2012).
- ³ M. Greiner, O. Mandel, T. Esslinger, T. W. Hänsch, and I. Bloch, *Nature* **415**, 39 (2002).
- ⁴ I. Bloch, J. Dalibard, and W. Zwerger, *Rev. Mod. Phys.* **80**, 885 (2008).
- ⁵ G. Zimmerli, G. Mistura, and M. H. W. Chan, *Phys. Rev. Lett.* **68**, 60 (1992).
- ⁶ A. Casey, H. Patel, J. Nyéki, B. P. Cowan, and J. Saunders, *Phys. Rev. Lett.* **90**, 115301 (2003).
- ⁷ M. Neumann, J. Nyéki, B. Cowan, and J. Saunders, *Science* **317**, 1356 (2007).
- ⁸ J. Nyéki, A. Phillis, A. Ho, D. Lee, P. Coleman, J. Parpia, B. Cowan, and J. Saunders, *Nature Physics* **13**, 455 (2017).
- ⁹ G. A. Csáthy, J. D. Reppy, and M. H. W. Chan, *Phys. Rev. Lett.* **91**, 235301 (2003).
- ¹⁰ P. A. Crowell, F. W. Van Keuls, and J. D. Reppy, *Phys. Rev. Lett.* **75**, 1106 (1995); *Phys. Rev. B* **55**, 12620 (1997).
- ¹¹ D. J. Bishop and J. D. Reppy, *Phys. Rev. Lett.* **40**, 1727 (1978); *Phys. Rev. B* **22**, 5171 (1980).
- ¹² J. D. Reppy, *J. Low Temp. Phys.* **87**, 205 (1992).
- ¹³ K. Shirahama, M. Kubota, S. Ogawa, N. Wada, and T. Watanabe, *Phys. Rev. Lett.* **64**, 1541 (1990).
- ¹⁴ P. A. Crowell and J. D. Reppy, *Physical Review B* **53**, 2701 (1996).
- ¹⁵ M. H. W. Chan, A. W. Yanof, and J. D. Reppy, *Phys. Rev. Lett.* **32**, 1347 (1974).
- ¹⁶ T. E. Washburn, J. E. Rutledge, and J. M. Mochel, *Phys. Rev. Lett.* **34**, 183 (1975).
- ¹⁷ M. P. A. Fisher, P. B. Weichman, G. Grinstein, and D. S. Fisher, *Phys. Rev. B* **40**, 546 (1989).
- ¹⁸ T. Giamarchi, P. L. Doussal, and E. Orignac, *Phys. Rev. B* **64**, 245119 (2001).
- ¹⁹ A. Golov and F. Pobell, *Phys. Rev. B* **53**, 12647 (1996).
- ²⁰ S. Brunauer, P. H. Emmett, and E. Teller, *J. Am. Chem. Soc.* **60**, 309 (1938).
- ²¹ E. P. Barrett, L. G. Joyner, and P. P. Halenda, *J. Am. Chem. Soc.* **73**, 373 (1951).
- ²² Y. Negishi, and K. Shirahama, unpublished.
- ²³ M. Hieda, T. Nishino, M. Suzuki, N. Wada, and K. Torii, *Phys. Rev. Lett.* **85**, 5142 (2000).
- ²⁴ C. Enss and S. Hunklinger, *Low-Temperature Physics* (Springer, 2005).
- ²⁵ R. H. Tait and J. D. Reppy, *Phys. Rev. B* **20**, 997 (1979).
- ²⁶ A. S. Nowick and B. S. Berry, *Anelastic Relaxation in Crystalline Solids* (Academic Press, New York and London, 1972).
- ²⁷ M. Boninsegni, *J. Low Temp. Phys.* **159**, 441 (2010).
- ²⁸ K. Yamamoto, H. Nakashima, Y. Shibayama, and K. Shirahama, *Phys. Rev. Lett.* **93**, 075302 (2004).
- ²⁹ N. Wada, T. Matsushita, M. Hieda, and R. Toda, *Journal of Low Temperature Physics* **157**, 324 (2009).
- ³⁰ R. Yu, L. Yin, N. S. Sullivan, J. S. Xia, C. Huan, A. Paduan-Filho, N. F. Oliveira Jr, S. Haas, A. Steppke,

- C. F. Mielea, F. Weickert, R. Movshovich, E.-D. Mun, B. L. Scott, V. S. Zapf, and T. Roscilde, *Nature* **489**, 379 (2012).
- ³¹ E. Kim and M. H. W. Chan, *Science* **305**, 1941 (2004).
- ³² Y. Aoki, I. Iwasa, T. Miura, D. Takahashi, A. Yamaguchi, S. Murakawa, and Y. Okuda, *J. Phys. Soc. Jpn.* **83**, 084604 (2014).
- ³³ D. Y. Kim and M. H. W. Chan, *Phys. Rev. Lett.* **109**, 155301 (2012).
- ³⁴ H. J. Maris, *Phys. Rev. B* **86**, 020502 (2012).